RF3 Induces Ribosomal Conformational Changes Responsible for Dissociation of Class I Release Factors

Haixiao Gao,[1,7] Zhihong Zhou,[2,7] Urmila Rawat,[3] Chenhui Huang,[4] Lamine Bouakaz,[4] Chernhoe Wang,[2] Zhihong Cheng,[2] Yuying Liu,[2] Andrey Zavialov,[4] Richard Gursky,[1] Suparna Sanyal,[4] Måns Ehrenberg,[4,*] Joachim Frank,[1,5,*] and Haiwei Song[2,6,*]

[1] Howard Hughes Medical Institute, Health Research, Inc. at the Wadsworth Center, Empire State Plaza, Albany, NY 12201-0509, USA
[2] Laboratory of Macromolecular Structure, Institute of Molecular and Cell Biology, 61 Biopolis Drive, Proteos, Singapore 138673
[3] Howard Hughes Medical Institute, University of Michigan School of Medicine, 1150 West Medical Ctr. Drive, Ann Arbor, MI 48109, USA
[4] Department of Cell and Molecular Biology, Uppsala University, BMC, Box 596, S-75124, Uppsala, Sweden
[5] Department of Biomedical Sciences, State University of New York at Albany, Empire State Plaza, Albany, NY 12201-0509, USA
[6] Department of Biological Sciences, National University of Singapore, 14 Science Drive, Singapore 117543
[7] These authors contributed equally to this work.
*Correspondence: ehrenberg@xray.bmc.uu.se (M.E.), joachim@wadsworth.org (J.F.), haiwei@imcb.a-star.edu.sg (H.S.)
DOI 10.1016/j.cell.2007.03.050

SUMMARY

During translation termination, class II release factor RF3 binds to the ribosome to promote rapid dissociation of a class I release factor (RF) in a GTP-dependent manner. We present the crystal structure of *E. coli* RF3•GDP, which has a three-domain architecture strikingly similar to the structure of EF-Tu•GTP. Biochemical data on RF3 mutants show that a surface region involving domains II and III is important for distinct steps in the action cycle of RF3. Furthermore, we present a cryo-electron microscopy (cryo-EM) structure of the posttermination ribosome bound with RF3 in the GTP form. Our data show that RF3•GTP binding induces large conformational changes in the ribosome, which break the interactions of the class I RF with both the decoding center and the GTPase-associated center of the ribosome, apparently leading to the release of the class I RF.

INTRODUCTION

Protein synthesis is in all organisms terminated by a class I release factor (RF) binding to a ribosome whose A site is programmed with a stop codon and whose P site is bound with peptidyl-tRNA. The bacterial class I RFs, RF1 and RF2, recognize the stop codons UAG/UAA and UGA/UAA, respectively (Scolnick et al., 1968), while the single eukaryotic class I RF eRF1 recognizes all three stop codons (Frolova et al., 1994). Class I RFs release newly synthesized proteins from the ribosome by triggering

hydrolysis of the ester bond in peptidyl-tRNA, presumably through contact between the universally conserved GGQ motif (Kisselev et al., 2003) and the peptidyl-transfer center (PTC) of the ribosomal 50S subunit (Nakamura and Ito, 2003). Genetic analysis has identified highly conserved tripeptide motifs in the bacterial class I RFs, which are directly involved in stop codon recognition in the decoding center (DC) of the small ribosomal subunit (Ito et al., 2000). The crystal structures of RF1 and RF2 have a compact, "closed" form, with distances between the codon recognition and GGQ motifs that are much shorter than the DC-PTC distance (Vestergaard et al., 2001; Shin et al., 2004). However, cryo-EM (Rawat et al., 2003, 2006; Klaholz et al., 2003) and recent X-ray crystallographic studies (Petry et al., 2005) show that ribosome-bound RF1 and RF2 possess similar "open" conformations, distinguished from the closed crystal forms of the isolated factors by large domain movements. These open conformations grant simultaneous access of the codon recognition and GGQ motifs to the DC and PTC, respectively. A recent small-angle X-ray scattering study revealed that RF1 in solution adopts a similar open configuration as ribosome-bound RF1 (Vestergaard et al., 2005), suggesting that the functional relevance of the crystal forms of RF1 and RF2 may be confined to the methylation of the Gln in the GGQ motif by the methyl-transferase PrmC (Graille et al., 2005).

The class II RFs, eRF3 in eukaryotes (Stansfield et al., 1995; Zhouravleva et al., 1995) and RF3 in bacteria (Grentzmann et al., 1994; Mikuni et al., 1994), are small GTPases. The function of RF3 is to remove RF1 or RF2 from the ribosomal A site after peptide release from the peptidyl-tRNA in the P site (Freistroffer et al., 1997). RF3 is one of the four major GTPases that participate in mRNA translation, with the other ones being initiation
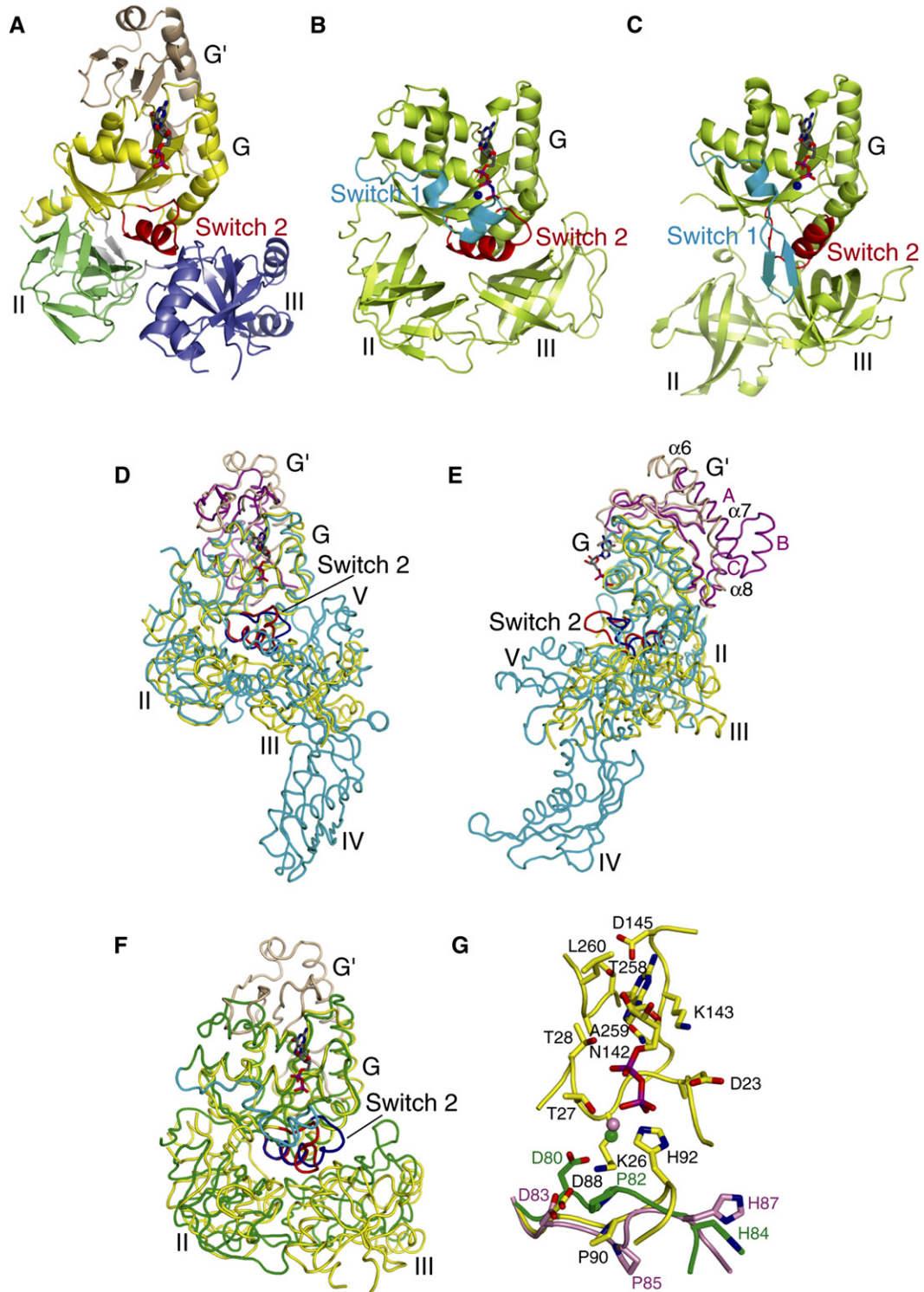
Figure 1. Crystal Structure of RF3•GDP and Its Comparison with Other Translational GTPases

(A) RF3•GDP, (B) EF-Tu•GTP (Kjeldgaard et al., 1993; 1EFT), and (C) EF-Tu•GDP (Song et al., 1999; 1EFC). Ribbon diagrams are drawn with G domain in the same orientation. Domains G′, G, II, and III of RF3•GDP are colored in wheat, yellow, lime green, and light blue, respectively, with the linker regions between domains in light gray. Switch 1 and 2 regions are colored in cyan and red, respectively. Bound nucleotide is shown as stick model, and Mg^{2+} ion is shown as a sphere.

(D, E, and F) Superposition of G domain of RF3•GDP with those of EF-G•GDP and EF-Tu•GTP. G′ domain of RF3•GDP, wheat; the rest of RF3•GDP, yellow; G′ domain of EF-G•GDP, pink; the rest of EF-G•GDP, cyan; EF-Tu•GTP, green; switch 1 of EF-G•GTP, cyan; switch 2 of

factor 2 (IF2), elongation factor Tu (EF-Tu), and elongation factor G (EF-G). Various studies have indicated that the G domains of these GTPases interact with the ribosome at a conserved site near the sarcin-ricin loop (SRL), and it is believed that this interaction is responsible for their ribosome-dependent GTPase activities (Stark et al., 1997; Agrawal et al., 1998; La Teana et al., 2001; Klaholz et al., 2004; Allen et al., 2005).

During its working cycle, RF3 enters the ribosome in complex with GDP (Zavialov et al., 2001). This binding event results in rapid exchange of GDP for GTP, provided that there is a class I RF in the A site and a deacylated tRNA in the P site (Zavialov et al., 2002). Separately, RF3, in complex with the noncleavable GTP analog GDPNP and RF1/RF2, has high affinity to the posttermination ribosome, but RF1/RF2 and RF3•GDPNP destabilize each other's binding to the posttermination ribosome with a deacylated P-site tRNA so that the presence of RF3•GTP is expected to greatly accelerate the dissociation of RF1/RF2 (Zavialov et al., 2001). From these observations it was postulated that GDP-to-GTP exchange on RF3 requires formation of a ribosome structure with high affinity to RF3•GTP (Zavialov et al., 2002). Until now, no structural information has been available for RF3 in support of this concept. For EF-G and IF2, large conformational changes of the ribosome have indeed been observed in conjunction with the removal of the peptide from the P-site-bound tRNA, characterized as a ratchet-like rotation of the 30S subunit relative to the 50S subunit (Frank and Agrawal, 2000; Valle et al., 2003; Allen et al., 2005). At the end of the RF3 working cycle, class I RF dissociation is followed by rapid hydrolysis of GTP on RF3 and swift release of RF3•GDP from the ribosome (Zavialov et al., 2001, 2002).

Recently, Klaholz et al. (2004) reported a cryo-EM study of RF3 in complex with GDPNP when present in a peptide-free release complex (RC; a complex consisting of the ribosome with a stop codon in the A site and a peptidyl-tRNA in the P site). Surprisingly, interpreted from two density maps at resolutions of 24 Å and 25 Å, the complex was seen in two states that differed in the conformations of both the ribosome and RF3, as well as in the location of tRNA. The fact that RF3 in complex with GDPNP is known to bind very stably to the peptide-free RC (Zavialov et al., 2001) raises the question whether the structures obtained by Klaholz et al. (2004) represent RF3 in the authentic GTP form.

Here we describe the crystal structure of *E. coli* RF3 in the GDP-bound state. It has three distinct domains and is remarkably similar in conformation to the crystal structure of EF-Tu•GTP. Moreover, we present a cryo-EM density map of ribosome-bound RF3•GDPNP. Docking the crystal structure of RF3•GDP into the density map of the

ribosome-bound RF3•GDPNP reveals that the binding of RF3•GDPNP leads to large conformational changes of the ribosome, which cause rapid dissociation of the class I RFs. These results, together with in vitro studies of RF3 mutants identified from the crystal structure of RF3•GDP, have now allowed a structural interpretation of previous biochemical data regarding RF3's mode of action (Zavialov et al., 2001, 2002; Zavialov and Ehrenberg, 2003).

RESULTS

Crystal Structure of RF3•GDP
The polypeptide chain of RF3•GDP is folded into three distinct domains (Figure 1A). Domain I (residues 3–278) is composed of a classic GTPase domain (G domain) and an "EF-G-like" G′ subdomain (Laurberg et al., 2000; Czworkowski et al., 1994). Domain I is connected to domain II (residues 294–387) by a peptide stretch with a small antiparallel β sheet in the middle (residues 279–293). Domain II forms a β-barrel structure as observed in EF-Tu (Song et al., 1999), eRF3 (Kong et al., 2004), and EF-G (Czworkowski et al., 1994). Domain II is connected to domain III (residues 391–529) by a short peptide linker. Domain III, composed of a central β-barrel flanked by two α helices, may represent a novel fold since no structural homolog was found in a Dali search.

Comparison of RF3•GDP and EF-G•GDP
Sequence analysis suggests the structures of RF3 and EF-G to be similar (Kisselev and Buckingham, 2000). To verify this prediction, we compared the crystal structure of RF3•GDP with that of a His573Ala mutant of EF-G (Laurberg et al., 2000). Superposition of the RF3•GDP domains G and G′, including the switch 2 region and the β-meander in the G′ subdomain, onto the corresponding EF-G•GDP domains, reveals great core domain similarity between the two translation factors (root-mean-square deviation (rmsd) = 1.5 Å; Figure 1D). There are, however, also notable differences between the two structures. First, helix α6 of G′ domain in RF3•GDP has no counterpart in EF-G•GDP. Second, helix α7 of RF3•GDP and the corresponding helix A of EF-G•GDP have distinct conformations with relative shifts of the equivalent Cα atoms up to 7 Å. Third, while helix α8 of RF3•GDP matches part of helix C of EF-G•GDP, helix B of EF-G•GDP has no counterpart in RF3•GDP (Figure 1E). These structural differences are in line with sequence differences in these regions of the two molecules (Figure S1).

Domain II of RF3•GDP and EF-G•GDP are quite similar, with an rmsd of 1.4 Å as estimated by superposition of the two domains. When G domain of RF3•GDP is superposed on that of EF-G•GDP, the orientations of domain II differ by only 13° (Figure 1D). Notably, the switch 1 region is

RF3•GDP, red; and switch 2 regions of EF-G•GDP and EF-Tu•GTP, blue. The orientations of (D) and (E) are related by a 90° rotation around y axis.
(G) Nucleotide-binding sites of RF3•GDP. RF3•GDP is in yellow; a portion of the switch 2 region is in green and pink for EF-Tu•GDP and EF-G•GDP, respectively.

disordered in both RF3•GDP and EF-G•GDP, and beyond domain II there is no structural similarity between the two molecules (Figure 1D).

The Structures of RF3•GDP and EF-Tu•GTP Are Similar

The tertiary structure of RF3•GDP is distinct from that of EF-Tu•GDP (Figure 1C) but is markedly similar to that of EF-Tu•GDPNP (EF-Tu•GTP; Figure 1B). The rmsd for the superposed domains I and II of RF3•GDP and EF-Tu•GDPNP is only 1.6 Å, and their switch 2 regions are strikingly similar (Figure 1F). The switch 1 region of RF3•GDP is disordered, but the structural similarities of the switch 2 regions and the whole G domains of EF-Tu•GTP and RF3•GDP suggest similar conformations also for their switch 1 regions. There is, in contrast, no match between domain III of RF3•GDP and EF-Tu•GTP due to their distinct overall folds (Figure 1F).

The Guanine Nucleotide-Binding Site of RF3•GDP

The interactions of the guanine moiety, the ribose ring, and the α-phosphate of GDP with the RF3 protein residues are very similar to the GDP interactions for EF-Tu (Song et al., 1999), EF-G (Laurberg et al., 2000), and eRF3 (Kong et al., 2004). A unique structural feature of RF3•GDP is the location of a conserved His92 residue in the switch 2 region, which at the sequence level corresponds to His84 for EF-Tu and His87 for EF-G (Figure S1). His92 is well defined in the electron density map and makes multiple contacts with the β-phosphate group of GDP (Figure 1G), suggesting that it contributes to the high-affinity binding of GDP to RF3 (Zavialov et al., 2001). In contrast, His84 in EF-Tu•GDP and His87 in EF-G•GDP are separated by ~10 Å from GDP (Figure 1G). As will be described below, His92 may also be involved in the triggering of GTP hydrolysis on ribosome-bound RF3, possibly by the same mechanism as proposed for His84 in EF-Tu (Kjeldgaard et al., 1993).

Mg^{2+} ions are considered to be essential cofactors for GTP hydrolysis in all G proteins. However, no Mg^{2+} ion was observed in the crystal structure of RF3•GDP, although the crystallization buffer contained 5 mM $MgCl_2$. In contrast, residues Asp50 and Asp80 of EF-Tu, corresponding to Asp58 and Asp88 of RF3, respectively (Figure S1), coordinate an Mg^{2+} ion in the crystal structures of both EF-Tu•GDP and EF-Tu•GTP (Kjeldgaard et al., 1993; Song et al., 1999). In the structure of RF3•GDP, Asp58 of switch 1 is disordered, and Asp88 of switch 2 is too far away to coordinate Mg^{2+} in its putative binding site (Figures 1A and 1G). It is, moreover, not unlikely that the presence of the positively charged His92 in RF3 further reduces the affinity of Mg^{2+} so that all these features could explain why Mg^{2+} is absent in the crystal but, by hypothesis, not in the native structure of RF3•GDP.

Biochemical Analysis of RF3 Mutants

Mapping of the sequence conservation shared by prokaryotic RF3 proteins on the surface of the crystal structure of RF3•GDP reveals two conserved patches. One is in the guanine nucleotide-binding region, including His92, and another in the interface between domains II and III (Figure 2A). To clarify the functional roles of these conserved surface regions, the RF3 variants H311A, R312A, E396A, Q445A, V448A, R452A, E456A, and Y457A were created by site-directed mutagenesis, expressed in *E. coli*, and purified to homogeneity. Mutation of His92 to Ala, Asn, or Asp either inhibited protein expression or resulted in an insoluble protein. However, a highly soluble double mutant His92Ala Pro90Gln (H92A P90Q) and, as a control, a single P90Q mutant could be expressed and purified.

We studied the ability of the wild-type and mutated variants of RF3 to accelerate recycling of RF1 or RF2 during termination on a RC containing an MFTI tetrapeptidyl-tRNA^{Ile} in the P site and a UAA stop codon in the A site. In these experiments, the ribosomes were present in excess, and each class I release factor had to recycle many times for complete termination (Freistroffer et al., 1997; Zavialov et al., 2001). We found an approximately 10-fold acceleration of recycling of both RF1 and RF2 by wild-type RF3. The recycling activities of the R312A, E396A, Q445A, and V448A mutants were similar to, or slightly lower than, those of wild-type RF3. The E456A and Y457A mutants had significantly, and the H311A and R452A mutants had strongly, reduced recycling activities compared to those of wild-type RF3. The recycling activity of the H92A P90Q double mutant was virtually zero, while the single P90Q mutation had an insignificant effect on the recycling activity (Figure 2B; Table S1).

The RF3 mutants H311A, R452A, and H92A P90Q, with strongly reduced recycling activities, were subjected to further studies relating to their guanine nucleotide-binding affinities and GDP exchange rates off, as well as on, RC. From nitrocellulose-filter binding (Zavialov et al., 2001), the dissociation equilibrium constants (K_{D-GDP}) for GDP binding to free RF3 were estimated as 5.6 nM (wild-type), 6.7 nM (H311A), 6.6 nM (R452A), and 18 nM (H92A P90Q). In experiments where radio-labeled GDP was chased from RF3 by unlabeled and repurified GTP, the ratio K_{D-GTP}/K_{D-GDP} between the dissociation equilibrium constants for GTP (K_{D-GTP}) and GDP (K_{D-GDP}) was estimated for each one of these RF3 mutants. The ratios for the wild-type, H311A, and R452A RF3 variants were similar and about 2-fold larger than the ratio for the H92A P90Q double mutant (Table S2; Figure S2).

The rates of GDP exchange for these mutants were estimated from stopped-flow experiments in which a solution with RF3-bound mant-GDP was rapidly mixed with a solution containing native GDP followed by recording of the time-dependent fluorescence decrease (Moore et al., 1992; Remmers et al., 1994). In line with the estimates for the equilibrium dissociation constant, the GDP dissociation rate constants were similar for the wild-type (0.036 s^{-1}), H311A (0.036 s^{-1}), and R452A (0.032 s^{-1}) variants and were a little more than 2-fold larger for the H92A P90Q (0.080 s^{-1}) variant and a little less than 2-fold larger for the P90Q (0.060 s^{-1}) single mutant. Very similar rate
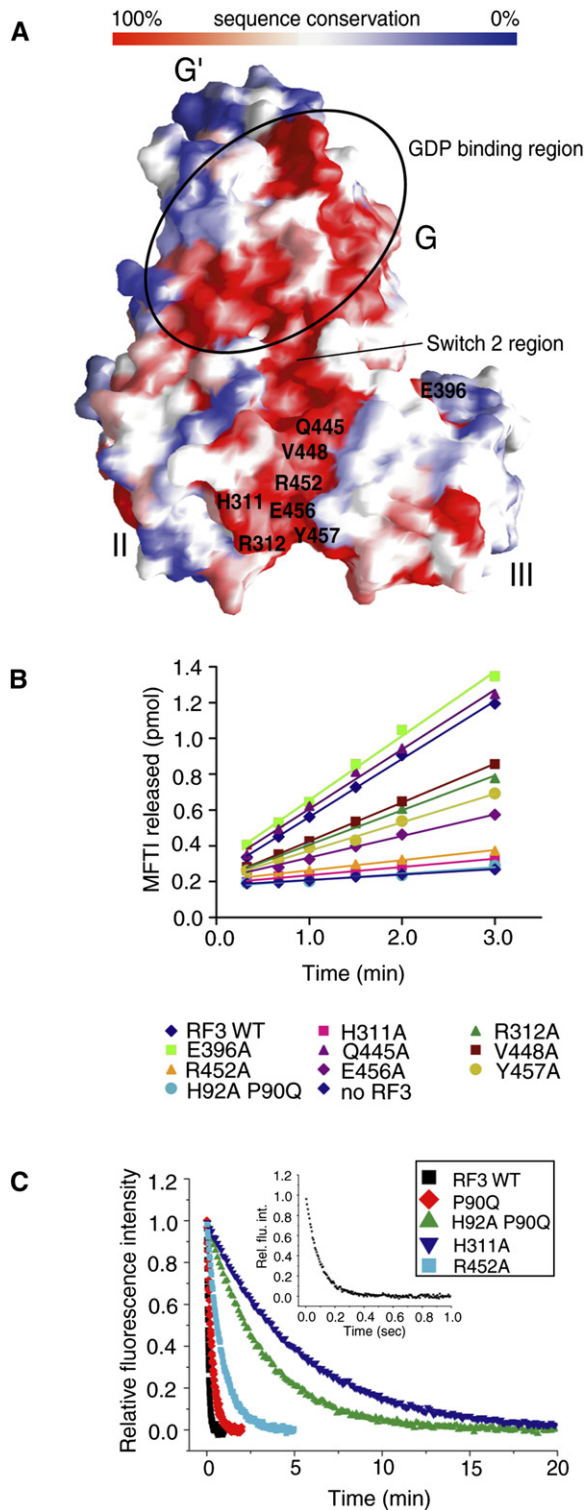
Figure 2. Effects of Mutations in the Conserved Regions of RF3

(A) Molecular surface of RF3•GDP (same view as in Figure 1A) showing regions of high to low sequence conservation shared by the prokaryotic RF3 proteins.

constants for GDP dissociation from these RF3 variants were estimated by nitrocellulose-binding experiments in which radio-labeled GDP was chased from RF3 by unlabeled GDP (data not shown).

We used stopped-flow to study also the rates of mant-GDP exchange for native GDP when solutions of mant-GDP bound RF3 variants were rapidly mixed with a solution of RF2-containing RC. The effective GDP dissociation rate constant was largest for wild-type RF3 (10.5 s^{-1}) and factors of 50, 9, or about 30 smaller for the H311A (0.19 s^{-1}), R452A (1.2 s^{-1}) and H92A P90Q (0.31 s^{-1}) variants, respectively. The effective GDP dissociation rate constant for the single P90Q mutant (5.6 s^{-1}) was just 2-fold smaller than for the wild-type RF3, suggesting that the greatly reduced GDP exchange rate by the H92A P90Q mutations was mainly due to the H92A, rather than to the P90Q alteration (Figure 2C; Table S2).

Reconstruction of the Peptide-free RC Bound with RF3

The above described in vitro system for mRNA translation (Zavialov et al., 2001) was used to prepare RCs. Subsequent addition of RF3, GDPNP, and puromycin–to remove the tetrapeptide from the P-site tRNA–led to a stable structure of the peptide-free RC bound with RF3 in the GTP form (henceforth to be referred to as RF3-bound RC). This complex represents an intermediate state of termination, i.e., after dissociation of the class I RF and before GTP hydrolysis and dissociation of RF3, and we obtained its structure by using cryo-EM and single-particle reconstruction (see Experimental Procedures). The EM density map exhibits the typical features of the 70S ribosome, with two additional densities (Figures 3A and 3B). One is attributed to tRNA with its anticodon in the P site of the 30S ribosomal subunit and its CCA end in the E site of the 50S ribosomal subunit, i.e., a hybrid P/E-site tRNA. The other density is attributed to RF3 and appears in the highly conserved factor-binding region at the entrance of the ribosomal intersubunit surface, where it contacts both the small and large ribosomal subunits.

Docking of Atomic Structures into the EM Density Maps

To obtain an atomic model of the RF3-bound RC in the GTP form, we docked the crystal structures of the *E. coli* 70S ribosome (Schuwirth et al., 2005) and RF3•GDP into our EM density map using real-space refinement (Chapman, 1995; Gao et al., 2003). Comparison of the crystal structure of RF3•GDP and the EM density of RF3 in the GTP form indicates that the two structures are

(B) Effects of RF3 mutations on the recycling rates of RF2. The tetrapeptide (MFTI) released from the RC (50 nM) as a result of recycling of RF2 (1.2 nM) in the presence of RF3 or its mutants in excess (200 nM) is plotted against time.

(C) Effect of RF3 mutations on the rate of GDP exchange monitored by the decrease of mant-GDP fluorescence at 440 nm as mant-GDP from RF3-mant-GDP complex (1 μM) was chased by unlabeled GDP (0.2 mM) in the presence of RC (200 nM) and RF2 (1 μM).
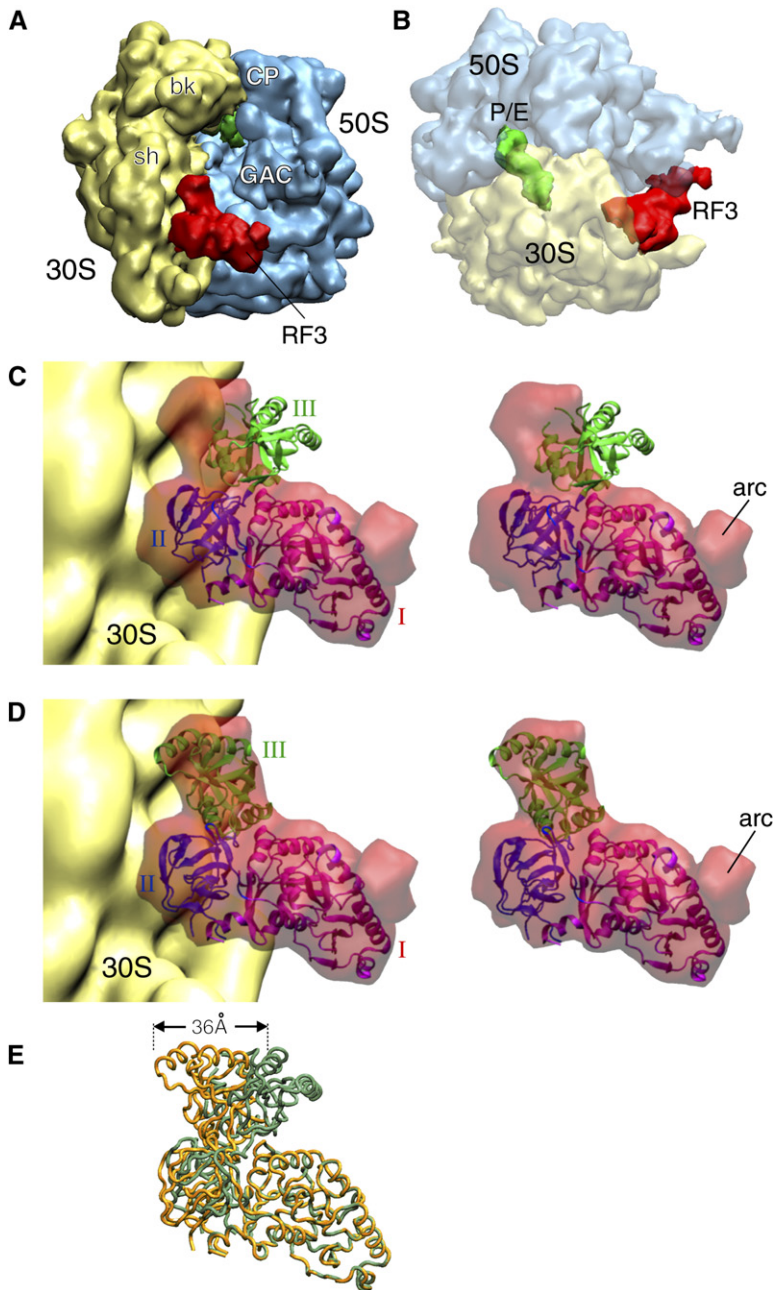
Figure 3. Peptide-free RC Bound with RF3•GDPNP

(A) Side view.

(B) Top view. RF3 (red) is located at the entrance of the intersubunit space between the 30S (yellow) and the 50S (blue) ribosomal subunits. The tRNA (green) is in the hybrid P/E site. bk indicates beak; sh indicates shoulder; CP indicates central protuberance; GAC indicates GTPase-associated center; P/E indicates hybrid P/E-site tRNA; and RF3 indicates release factor 3.

(C) Stereo view of crystal structure of RF3•GDP superposed with the density of RF3•GDPNP.

(D) Stereo view of model of RF3•GDPNP.

(E) Superposition of crystal structure of RF3•GDP (green) and model of RF3•GDPNP (yellow). In (C) and (D), EM density of RF3•GDPNP is in semitransparent red, and atomic structures of RF3 are colored as: domain I, red; domain II, blue; and domain III, green.

significantly different (CC = 0.42). While domain I of the crystal structure directly fits into the EM density map, domains II and III require additional arrangement (Figure 3C). Thus, the crystal structure of RF3•GDP was docked into the EM density as three rigid pieces by allowing relative domain movement in the factor, thereby increasing the CC to 0.72 (Figure 3D). In addition, the 70S ribosome was fitted (CC = 0.72) as multiple rigid pieces according to a previously developed rigid-body assignment (Gao et al., 2003; also see Experimental Procedures).

Besides the RF3-bound RC in the GTP form, docking was also applied to the EM density maps of functionally

important ribosomal termination complexes from previous studies (Rawat et al., 2003, 2006), including (i) a control density map of the RC, (ii) RF1-bound RC, and (iii) RF2-bound RC (both "after" peptidyl-tRNA hydrolysis). The final fitting statistics for all the complexes (CC > 0.7, R factor ∼0.2) shows good overall fitting of the structural models into their EM density maps (Table S3).

Molecular Interpretation of RF3's GTPase Activity
Starting from the crystal structure of RF3•GDP, the model of RF3 in the GTP form was obtained by large translational and rotational movements of both domains II and III relative
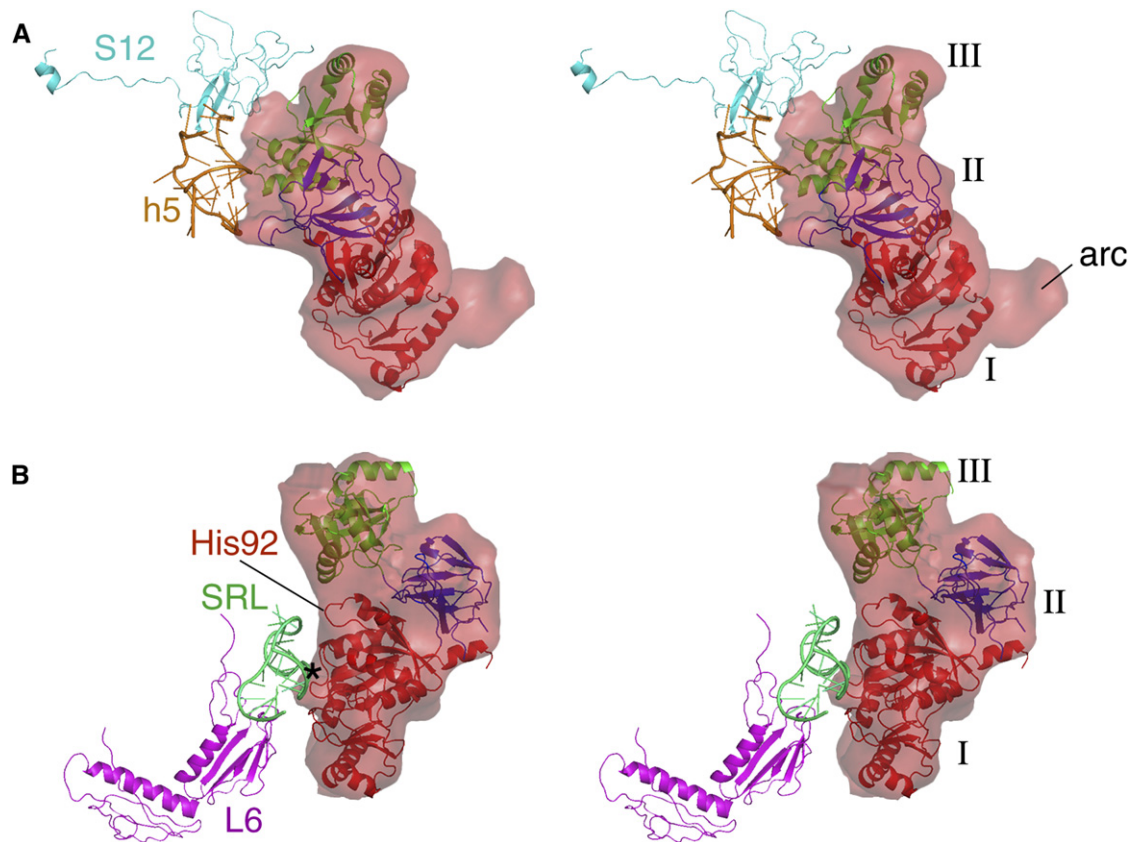
Figure 4. Molecular Interactions of RF3•GDPNP with the 70S Ribosome
Stereo views showing interactions of (A) domains II and III of RF3 with helix 5 (orange) and protein S12 (cyan) from the 30S subunit and (B) domain I of RF3 with SRL (teal) and protein L6 (purple) from the 50S subunit. The guanine nucleotide-binding site is indicated by an asterisk. S12 indicates protein S12; h5 indicates helix 5; SRL indicates sarcin-ricin loop; L6 indicates protein L6; and His 92 indicates residue His92.

to domain I. The maximum displacement of 36 Å occurs in domain III near the C-terminal (Figure 3E) and is similar to the domain IV movement from the GDP form of free EF-G to its ribosome-bound GTP form (Valle et al., 2003).

The interaction of RF3 in the GTP form with the peptide-free RC involves all three domains of RF3, as well as the 30S and 50S subunits (Figure 4). RF3 binds to the 30S subunit in the region of helix 5 of 16S rRNA and ribosomal protein S12, a region known as a conserved binding site for several protein factors (Spahn et al., 2001; Valle et al., 2002). Helix 5 interacts with domains II and III of RF3, and protein S12 forms extensive contacts with domain III. In the 50S subunit, as expected, the G domain of RF3 interacts with the SRL and protein L6, consistent with the G domain locations of other translational GTPases. The guanine nucleotide-binding site, located near Lys143 and Leu260 in domain I of RF3 (Figure 1G), is less than 10 Å away from, and thereby closest to, the SRL (Figure 4B). The conserved residue His92 in the switch 2 region also lies close to the SRL (Figure 4B), which is important for GDP exchange on ribosome-bound RF3 (Table S2) and essential for the recycling function of this factor (Table S1).

While the EM density of RF3 in the GTP form accommodates all three domains from the crystal structure quite well, there is a partial "arc-like" density appearing at the far end of domain I (Figure 4), which cannot be fitted with the crystal structure. Similar arc-like densities have been spotted in cryo-EM reconstructions of ribosome-bound forms of the other three translational GTPases: EF-G (Agrawal et al., 1998, 1999), EF-Tu (Stark et al., 1997; Valle et al., 2002), and IF2 (Allen et al., 2005). These arcs were interpreted as connections between the respective factor's G (or G') domain and either the N-terminal domain (NTD) of L11 (Agrawal et al., 2001) or the C-terminal domain (CTD) of L7/L12 (Allen et al., 2005).

RF3-Induced Conformational Changes of the Ribosome

To investigate the RF3-induced conformational changes of the ribosome, we compared the density map of the RF3-bound RC from this study with the previous maps of the RC itself and of RC bound with RF1/RF2 (Rawat et al., 2003, 2006). Superposition of these maps immediately revealed significant conformational changes in both the small and large ribosomal subunits of the RF3-bound
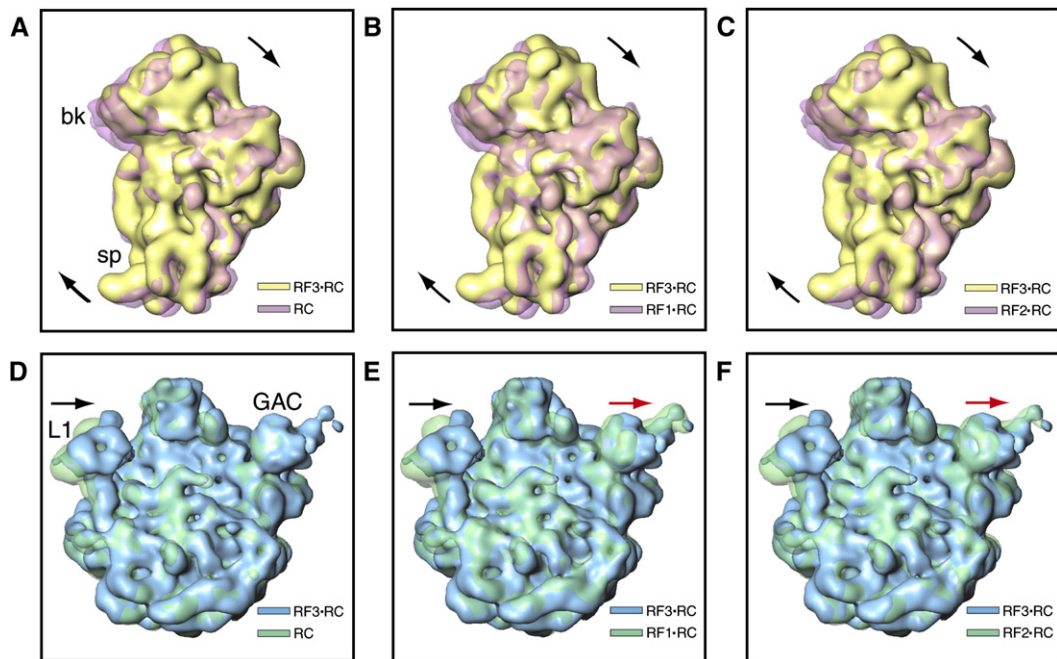
Figure 5. Ribosomal Conformational Changes upon Binding of RF3•GDPNP

(A–C) Comparison of the 30S subunit of RF3-bound RC (solid yellow) with the 30S subunits (semitransparent purple) of (A) RC, (B) RF1-bound RC, and (C) RF2-bound RC. The ratchet-like rotation is indicated by the pair of arrows.

(D–F) Comparison of the 50S subunit of RF3-bound RC (solid blue) with the 50S subunits (semitransparent green) of (D) RC, (E) RF1-bound RC, and (F) RF2-bound RC. The inward movement of the L1 stalk and the outward movement of the GAC in the RF3-bound RC are marked by black and red arrows, respectively.

RC. As shown in Figure 5, compared with the other three density maps, in the RF3-bound RC, the 30S subunit shows a 10° ratchet-like rotation, while the L1 stalk in the 50S subunit flexes about 20° toward the central protuberance (CP). Both conformational changes are virtually identical to those observed previously in a ribosome complex with EF-G in the GTP form (Valle et al., 2003).

Besides the ratcheting motion and the flexing movement of the L1 stalk, binding of RF3 to the peptide-free RC also induces significant conformational changes in the GAC regions in the above four density maps (Figure 5). Recent studies showed that the binding of RF1/RF2 to the RC induces a 6 Å inward curling of the entire GAC region toward PTC (Rawat et al., 2006), which was suggested to promote the exchange of GDP to GTP in RF3 (Mora et al., 2003). It appears that the GAC in the RF3-bound RC is not in the same inward-curled position as in the maps of RF1- and RF2-bound RC. Instead, its GAC position matches with the one found in the density map of RC, indicating that the binding of RF3 in the GTP form to the peptide-free RC in fact *reverses* the movement of GAC that occurred upon binding of RF1 or RF2.

RF3-Induced Release of RF1 and RF2 from the Ribosome

In an attempt to identify the mechanism by which RF3 induces dissociation of class I release factors from the ribosome after peptide release, we first compared the ribosomal binding sites of RF3•GDPNP with those of RF1 and RF2. Positioning of the structural model of RF3•GDPNP into the EM density maps of RC bound with RF1 or RF2 (Rawat et al., 2003, 2006) clearly showed that there is no overlap between the ribosomal binding sites of RF3 and RF1/RF2 (Figure 6). The only possible interaction is between domain III of RF3 and domain I of RF1/RF2, as measured by the closest distance of 9 Å between Cα atoms. Considering the ratchet-like rotation in the 30S subunit upon binding of RF3 in the GTP form, the spatial location of RF3 is also affected. If we counteract the ratchet-like rotation by rotationally aligning the 30S ribosomal subunits, the relative positions between the RF3 and the two class I RFs are even more separated (Figure S3). Another comparison, with the recent *T. thermophilus* crystal structures of RF1 or RF2 bound to the ribosome (Petry et al., 2005), confirms that the two classes of RFs do not compete for a common ribosomal binding site (Figure S4).

To further elucidate the mechanism of the rapid dissociation of RF1 or RF2 promoted by RF3, we focus on the conformational changes that occur in the ribosome upon the binding of class I and class II RFs. Structural studies have shown that both class I RFs bind to three functionally important centers on the ribosome, i.e., the DC, the PTC, and the GAC, involving domains II, III, and I of the factors,
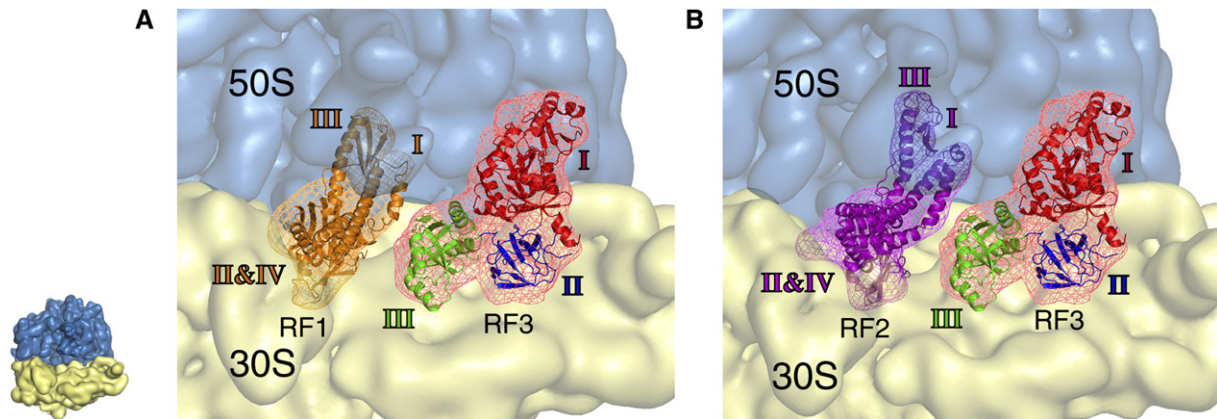
Figure 6. Relative Positions of RF1/RF2 and RF3 on the Ribosome

Density and model of RF3•GDPNP are placed into (A) RF1-bound RC (Rawat et al., 2006) and (B) RF2-bound RC (Rawat et al., 2003). Ribosomal subunits are shown in semitransparent blue (50S) and yellow (30S), respectively. Densities of RF1 (orange), RF2 (pink), and RF3 (red) are rendered in wire mesh, and structural models of RF1 (2FVO), RF2 (1GQE), and RF3•GDPNP (same color code as in Figure 4) are in ribbons.

respectively (Rawat et al., 2003, 2006; Petry et al., 2005). In order for RF1 or RF2 to dissociate from the ribosome, it is expected that the interactions between the factor and the ribosome in these regions are the first to be disrupted. Indeed, according to the atomic models of the ribosome obtained by real-space refinement fitting, upon binding of RF3•GDPNP, significant ribosomal conformational changes are observed in the regions of the DC and the GAC, two of the three known factor-binding sites (Figure S5). First, as we go from the RC bound with RF1 or RF2 to the peptide-free RC bound with RF3, the DC, riding with the ratchet-like motion of the 30S ribosomal subunit, moves away by 6 Å from the binding site with domain II of RF1 and RF2. Second, as described earlier, the different positions of the GAC, deduced from the maps of the RC bound with RF1/RF2 and the peptide-free RC bound with RF3, indicate a GAC movement away (∼6 Å) from the binding site with domain I of RF1/RF2. It is, we suggest, the RF3-induced interruption of this interaction between the GAC and the class I RF that promotes its rapid dissociation. As far as the PTC, the third binding site of RF1 and RF2, is concerned, no significant change was observed upon the binding of RF3 to the ribosome. It is likely that the interaction between the PTC and domain III of RF1/RF2 is only required for hydrolysis of the ester bond in peptidyl-tRNA. Once the polypeptide is released, such an interaction would no longer be required.

DISCUSSION

Based on our structural analyses and the new biochemical data, we propose a model for the RF3-mediated termination mechanism in which the prior binding of RF1 or RF2 to the RC induces the cleavage of polypeptide from the P-site tRNA and thereby "unlocks" the ribosome, in the sense (Valle et al., 2003) that the ratchet motion now becomes possible while it was blocked before.

First, RF3 in the GDP form binds to the ribosome with low affinity. Subsequently, the dissociation of GDP from RF3 is catalyzed by the RC containing a class I release factor. From sequence conservation mapping, we have identified a set of functionally important residues, including H311 and R452 in the domain II/III interface on the surface of RF3. When either H311 or R452 is changed to Ala, the RC-dependent, but not the spontaneous GDP-to-GDP, exchange rate on RF3 is greatly reduced (Table S2). These observations can be explained as being due to an H311- and R452-dependent stabilization of the guanine nucleotide-free form of RF3 with low affinity for GDP, which would promote rapid GDP dissociation from ribosome-bound RF3 (Freistroffer et al., 1997; Zavialov et al., 2001). In this scenario, the two mutations fail to stabilize the nucleotide-free form of RF3, thereby greatly reducing the dissociation rate of GDP, as observed (Figure 2C).

After dissociation of GDP, GTP rapidly binds to the guanine nucleotide-free state of RF3. This event induces conformational changes both in RF3, created by the extended movement of domains II and III, and in the ribosome, characterized by the ratchet-like movement of the small relative to the large subunit accompanied by movements of the L1 stalk and the GAC. Formation of this high-affinity complex between RF3•GTP and the peptide-free RC (Zavialov et al., 2001) breaks the interactions between the ribosome and RF1/RF2 in the region of DC and GAC, ultimately causing the release of RF1/RF2. Finally, GTP hydrolysis causes RF3 to switch back to its low-affinity GDP form, which triggers its rapid dissociation from the ribosome. Simultaneously, both the ratchet-like movement and the movement of L1 are reversed, which brings the ribosome back to the same conformation as seen in RC.

This second part of our model is strongly supported by the mutational study on the conserved residues located on the interface of domains II and III of RF3•GDP. Our kinetic data show that the H311A or R452A mutations
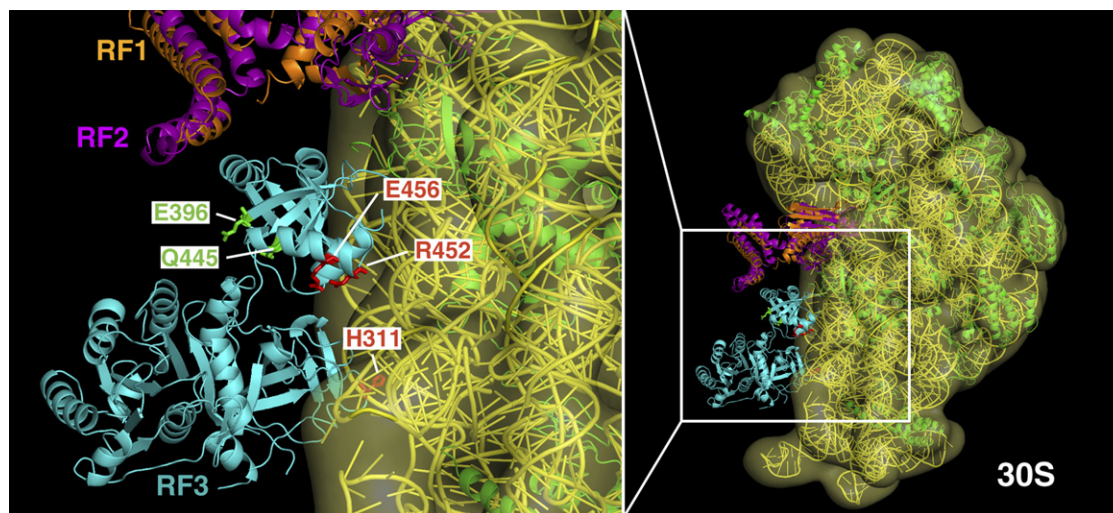
Figure 7. Structural Interpretation of the Mutation Study of RF3-Ribosome Interaction

The boundary of the EM density for the 30S subunit of the RF3-bound RC is shown by semitransparent contour mesh in yellow. Its atomic model (rRNA, yellow; protein, green) was obtained by real-space refinement. Atomic models of RF1 (orange), RF2 (pink), and RF3•GDPNP (cyan) are rendered in ribbons. Residues E456, R452, and H311 (red) appear near the 30S ribosomal binding site, and residues E396 and Q445 (green) are away from the 30S ribosomal binding site.

strongly (though to a different degree) reduce the GDP exchange rate for RC-bound RF3 (Table S2). However, these effects are far too small to account for the very large, virtually uniform increase in the total class I RF recycling time caused by these H311A or R452A mutations (Figure 2B; Table S1). From this fact we infer that the H311A and R452A mutations must affect two steps in the action cycle of RF3, i.e., (1) decreasing the rate of GDP dissociation from RF3 bound to a class I RF containing RC or (2) decreasing the rate of a subsequent rate-limiting step for class I RF recycling after peptide release. We note further that the E456A mutation moderately reduces the recycling activity of RF3, while the E396A and Q445A mutations do not have a significant effect on it (Figure 2B; Table S1). According to our structural model for ribosome-bound RF3 in the GTP form, residues H311, R452, and E456 are expected to be in direct contact with the 30S subunit (Figure 7). It is therefore conceivable that the mutations in these residues will interfere with the binding of RF3 in the GTP form to the ribosome, as well as with the induction of these ribosomal conformational changes, which we suggest are responsible for the RF3-induced rapid dissociation of RF1/RF2. In contrast, the locations of E396 and Q445 are *away* from the ribosomal binding site and exposed to the solvent (Figure 7). Evidently, these latter sites are not involved in ribosomal binding, nor do they have an impact on the recycling of RF1 and RF2.

Concerning the H92A P90Q double mutant of RF3, the RC-dependent GDP to GDP exchange rate is reduced 30-fold (Table S2), and the overall RF3 recycling activity is virtually zero (Figure 2B; Table S1). It is unlikely that these effects are primarily caused by perturbed interactions between RF3 and a class I RF or the ribosome. Instead, we

suggest that the H92A P90Q variant of RF3 is locked in a conformation similar to, but not identical with, the GDP form of wild-type RF3. Its failure to adopt the authentic guanine nucleotide-free form of RF3 on the ribosome explains, we suggest, why the ribosome-dependent GDP-to-GDP exchange rate is reduced 30-fold in relation to the wild-type rate (Table S2). The subsequent failure of H92A P90Q to adopt the authentic GTP form of wild-type RF3 would explain, following this hypothesis, why the class I RF recycling activity of the H92A P90Q RF3 mutant is virtually zero.

We have seen here how the binding of RF3•GDPNP to the peptide-free RC drives the ratchet-like conformational change of the ribosome, the swivel motion of the L1 stalk, and the movement of the deacylated tRNA from the P to the hybrid P/E site (Figures 3 and 5). It is noteworthy that these changes are very similar to the conformational changes previously observed in the case of EF-G•GDPNP binding to an unlocked ribosome (Valle et al., 2003). Besides, depending on their GTP and GDP forms, both RF3 and EF-G bind to the ribosome with high affinity in an extended conformation and with low affinity in the compact conformation. These structural similarities imply the existence of a general mechanism underlying both RF3-dependent termination and EF-G-dependent translocation in which the ratcheting motion in the ribosome plays a key role.

Compared with the previous cryo-EM study by Klaholz et al. (2004) in which the complex of RF3-bound RC was reported to assume two different conformations, the structure we present in this study not only demonstrates a significantly improved resolution but, more importantly, shows a stable, single conformation highly consistent

with the biochemical data. Furthermore, the newly solved X-ray structure of RF3 has now allowed us to build an authentic model of RF3 bound to RC in the GTP state and to describe an RF3-mediated termination mechanism that is strongly supported by the new biochemical data presented in this study. In contrast, the molecular interpretation of RF3 by Klaholz et al. (2004) was limited by the use of EF-G as a homolog and is now proven to be inaccurate by the X-ray structure that shows that the structural similarity between RF3 and EF-G is limited to domains I and II.

EXPERIMENTAL PROCEDURES

Structure Determination of RF3•GDP

SeMet MAD data were collected at three wavelengths on beamline BW7A at EMBL (Hamburg, Germany) using a MarCCD detector and processed with Mosflm (CCP4, 1994). Crystals belong to space group $P2_12_12_1$, with the cell parameters of a = 73.17 Å, b = 239.78 Å, and c = 69.68 Å, and contain two molecule per asymmetric unit (AU).

The structure of RF3•GDP was determined by MAD method. Heavy atom search and refinement were carried out using the SnB (Miller et al., 1994) and SHARP (De la Fortelle and Bricogne, 1997), respectively. About 80% of the final model was built automatically using ARP/wARP (Perrakis et al., 1999); the rest was built manually using O (Jones et al., 1991). The model was refined using CNS (Brunger et al., 1998) and REFMAC5 (Murshudov et al., 1997). Neither molecule A nor B of the AU contained Mg^{2+}, and each of them contained one GDP molecule, although the crystallization buffer contained 5 mM Mg^{2+} and lacked nucleotides. Residues 1–2, 39–69, 351–355, and 407–409 for molecule A and 38–69, 305–312, 350–354, and 405–408 for molecule B in the AU are disordered. The final refinement statistics are summarized in Table S4.

Site-Directed Mutagenesis and Recycling of RF1/RF2 by RF3

All the RF3 mutants were created using the QuickChange mutagenesis kit (Stratagene) and purified using same methods as wild-type RF3. These are H92A P90Q, H311A, R312A, E396A, Q445A, V448A, R452A, E456A, Y457A, and P90Q, respectively. The RC with a UAA stop codon in the A site and a MFTI-tRNA in the P site was prepared as described (Bouakaz et al., 2006), and the recycling of the release factors RF1 (5 nM) and RF2 (1.2 nM) on RC (50 nM) in the presence of excess wild-type (WT) or the mutant RF3s (200 nM) was done as described (Zavialov et al., 2001).

GDP Exchange on RF3

To study GDP exchange on wild-type RF3 and its mutants (H92A P90Q, P90Q, H311A, and R452A), 1 μM RF3 was incubated with 2 μM mant-GDP, a fluorescent derivative of GDP (Moore et al., 1992; Zhang et al., 2005), at 37°C for 10 min in a 1× Hepes-polymix buffer containing 10 mM Hepes, 5 mM magnesium acetate, 5 mM ammonium chloride, 95 mM potassium chloride, 0.5 mM calcium chloride, 8 mM putrescine, 1 mM spermidine, and 1 mM dithioerythritol. This complex was chased by 200 μM GDP in the absence or presence of 200 nM RC (fMet-UAA) preincubated with 1 μM RF2 at 37°C for 10 min. The rate of GDP exchange was monitored by measuring the decrease of mant-GDP fluorescence at 440 nm with time in a stopped-flow apparatus. In parallel, GDP exchange was also measured by nitrocellulose filter-binding assay using RF3·[³H]GDP complex (Zavialov et al., 2001).

Cryo-EM and Image Processing

RCs were prepared as described (Zavialov et al., 2001). Two micromolar RF3 was incubated with 0.5 mM GDPNP, and 0.16 μM RC was treated with 0.8 mM puromycin, both at 37°C for 10 min in polymix buffer. All the reaction components were mixed and incubated at 37°C for 5 min. Occupancy of RF3 on the ribosome was estimated

as 80% by nitrocellulose filter-binding of the RF3• [³H]-GDPNP•RC (Zavialov et al., 2001). The above reaction mixture was diluted to a ribosome concentration of 32 nM and transferred to cryo-grids in cold room at 4°C.

EM data were collected on a FEI Tecnai F20 at 200 kV with an electron dose of 20 e⁻/Å² and a magnification of 49,650×. Micrographs were digitized on a Zeiss/Imaging scanner (Z/I Imaging Corporation, Huntsville, Alabama) with a step size of 14 μm, corresponding to 2.82 Å on the object scale. Forty-five thousand particle images were subjected to the reference-based 3D reconstruction using SPIDER (Frank et al., 1996). Resolution of the refined and CTF-corrected density map is 15.5 Å or 9.7 Å, according to the Fourier Shell Correlation criterion, using cutoff value of 0.5 or 3σ, respectively. Fourier amplitudes were corrected using the X-ray solution scattering data as described (Gabashvili et al., 2000). Figures were prepared with IRIS EXPLORER (Numerical Algorithms Group, Downers Grove, IL), VMD (Humphrey et al., 1996), and PyMOL (DeLano Scientific, San Carlos, CA).

Real-Space Refinement

Docking was performed using real-space refinement implemented in RSRef (Chapman, 1995) and TNT (Tronrud et al., 1987). A multi-rigid-body refinement scheme was employed (Gao et al., 2003). RF3 was fitted as three rigid pieces according to the factor's domain divisions. The 70S ribosome (PDB entry: 2AVY/2AW4) was fitted as a total of 157 rigid pieces in which RNAs were divided according to their secondary structure (Gao et al., 2003), and each ribosomal protein was treated as single rigid piece.

Supplemental Data

Supplemental Data include Experimental Procedures, four tables, five figures, and one movie and can be found with this article online at http://www.cell.com/cgi/content/full/129/5/929/DC1/.

REFERENCES

Agrawal, R.K., Penczek, P., Grassucci, R.A., and Frank, J. (1998). Visualization of elongation factor G on the *Escherichia coli* 70S ribosome: the mechanism of translocation. Proc. Natl. Acad. Sci. USA *95*, 6134–6138.

Agrawal, R.K., Heagle, A.B., Penczek, P., Grassucci, R.A., and Frank, J. (1999). EF-G-dependent GTP hydrolysis induces translocation accompanied by large conformational changes in the 70S ribosome. Nat. Struct. Biol. *6*, 643–647.

Agrawal, R.K., Linde, J., Sengupta, J., Nierhaus, K.H., and Frank, J. (2001). Localization of L11 protein and elucidation of its involvement in EF-G-dependent translocation. J. Mol. Biol. *311*, 777–787.

Allen, G.S., Zavialov, A., Gursky, R., Ehrenberg, M., and Frank, J. (2005). The cryo-EM structure of a translation initiation complex from *Escherichia coli*. Cell *121*, 703–712.

Bouakaz, L., Bouakaz, E., Murgola, E.J., Ehrenberg, M., and Sanyal, S. (2006). The role of ribosomal protein L11 in class I release factor-mediated translation termination and translational accuracy. J. Biol. Chem. *281*, 4548–4556.

Brunger, A.T., Adams, P.D., Clore, G.M., DeLano, W.L., Gros, P., Grosse-Kunstleve, R.W., Jiang, J.-S., Nilges, N., Pannu, N.S., Read, R.J., et al. (1998). Crystallography and NMR system (CNS): A new software system for macromolecular structure determination. Acta Crystallogr. *D54*, 905–921.

CCP4. (1994). The CCP4 suite: programs for protein crystallography. Acta Crystallogr. *D50*, 760–763.

Chapman, M.S. (1995). Restrained real-space macromolecular atomic refinement using a new resolution-dependent electron-density function. Acta Crystallogr. *A51*, 69–80.

Czworkowski, J., Wang, J., Steitz, T.A., and Moore, P.B. (1994). The crystal structure of elongation factor G complexed with GDP, at 2.7 A resolution. EMBO J. *13*, 3661–3668.

De la Fortelle, E., and Bricogne, G. (1997). Maximum-likelihood heavy-atom parameter refinement for multiple isomorphous replacement and multiwavelength anomalous diffraction method. Meth. Enzymol. *276*, 472–494.

Frank, J., and Agrawal, R.K. (2000). A ratchet-like inter-subunit reorganization of the ribosome during translocation. Nature *406*, 318–322.

Frank, J., Radermacher, M., Penczek, P., Zhu, J., Li, Y., Ladjadj, M., and Leith, A. (1996). SPIDER and WEB: processing and visualization of images in 3D electron microscopy and related fields. J. Struct. Biol. *116*, 190–199.

Freistroffer, D., Pavlov, M.Y., MacDougall, J., Buckingham, R.H., and Ehrenberg, M. (1997). Release factor RF3 in E.coli accelerates the dissociation of release factors RF1 and RF2 from the ribosome in a GTP-dependent manner. EMBO J. *16*, 4126–4133.

Frolova, L., Le Goff, X., Rasmussen, H.H., Cheperegin, S., Drugeon, G., Kress, M., Arman, I., Haenni, A.L., Celis, J.E., Philippe, M., et al. (1994). A highly conserved eukaryotic protein family possessing properties of polypeptide chain release factor. Nature *372*, 701–703.

Gabashvili, I.S., Agrawal, R.K., Spahn, C.M.T., Grassucci, R.A., Frank, J., and Penczek, P. (2000). Solution structure of the *E.coli* 70S ribosome at 11.5 Å resolution. Cell *100*, 537–549.

Gao, H., Sengupta, J., Valle, M., Korostelev, A., Eswar, N., Stagg, S.M., Van Roey, P., Agrawal, R.K., Harvey, S.C., Sali, A., et al. (2003). Study of the structural dynamics of the *E. coli* 70S ribosome using real space refinement. Cell *113*, 789–801.

Graille, M., Heurgue-Hamard, V., Champ, S., Mora, L., Scrima, N., Ulryck, N., van Tilbeurgh, H., and Buckingham, R.H. (2005). Molecular basis for bacterial class I release factor methylation by PrmC. Mol. Cell *20*, 917–927.

Grentzmann, G., Brechemier-Baey, D., Heurgue, V., Mora, L., and Buckingham, R.H. (1994). Localization and characterization of the gene encoding release factor RF3 in Escherichia coli. Proc. Natl. Acad. Sci. USA *91*, 5848–5852.

Humphrey, W., Dalke, A., and Schulten, K. (1996). VMD - visual molecular dynamics. J. Mol. Graph. *14*, 33–38.

Ito, K., Uno, M., and Nakamura, Y. (2000). A tripeptide 'anticodon' deciphers stop codons in messenger RNA. Nature *403*, 680–684.

Jones, T.A., Zhou, J.Y., Cowan, S.W., and Kjeldgaard, M. (1991). Improved methods for building protein models in electron density maps and the location of errors in these models. Acta Crystallogr. *A47*, 110–119.

Kisselev, L., Ehrenberg, M., and Frolova, L. (2003). Termination of translation: interplay of mRNA, rRNAs and release factors? EMBO J. *22*, 175–182.

Kisselev, L.L., and Buckingham, R.H. (2000). Translational termination comes of age. Trends Biochem. Sci. *25*, 561–566.

Kjeldgaard, M., Nissen, P., Thirup, S., and Nyborg, J. (1993). The crystal structure of elongation factor EF-Tu from Thermus aquaticus in the GTP conformation. Structure *1*, 35–50.

Klaholz, B.P., Pape, T., Zavialov, A.V., Myasnikov, A.G., Orlova, E.V., Vestergaard, B., Ehrenberg, M., and van Heel, M. (2003). Structure of the Escherichia coli ribosomal termination complex with release factor 2. Nature *421*, 90–94.

Klaholz, B.P., Myasnikov, A.G., and van Heel, M. (2004). Visualization of release factor 3 on the ribosome during termination of protein synthesis. Nature *427*, 862–865.

Kong, C., Ito, K., Walsh, M.A., Wada, M., Liu, Y., Kumar, S., Barford, D., Nakamura, Y., and Song, H. (2004). Crystal structure and functional analysis of the eukaryotic class II release factor eRF3 from S. pombe. Mol. Cell *14*, 233–245.

La Teana, A., Gualerzi, C.O., and Dahlberg, A.E. (2001). Initiation factor IF 2 binds to the alpha-sarcin loop and helix 89 of Escherichia coli 23S ribosomal RNA. RNA *7*, 1173–1179.

Laurberg, M., Kristensen, O., Martemyanov, K., Gudkov, A.T., Nagaev, I., Hughes, D., and Liljas, A. (2000). Structure of a mutant EF-G reveals domain III and possibly the fusidic acid binding site. J. Mol. Biol. *303*, 593–603.

Mikuni, O., Ito, K., Moffat, J., Matsumura, K., McCaughan, K., Nobukuni, T., Tate, W., and Nakamura, Y. (1994). Identification of the prfC gene, which encodes peptide-chain-release factor 3 of Escherichia coli. Proc. Natl. Acad. Sci. USA *91*, 5798–5802.

Miller, R., Gallo, S.M., Khalak, H.G., and Weeks, C.M. (1994). *SnB*: crystal structure determination *via* shake-and-bake. J. Appl. Crystallogr. *27*, 613–621.

Moore, K.J., Lowe, P.N., and Eccleston, J.F. (1992). The kinetic mechanism of the GAP-activated GTPase of p21 ras. Philos. Trans. R. Soc. Lond. B Biol. Sci. *336*, 49–53.

Mora, L., Zavialov, A.V., Ehrenberg, M., and Buckingham, R.H. (2003). Stop codon recognition and interactions with peptide release factor RF3 of truncated and chimeric RF1 and RF2 from Escherichia coli. Mol. Microbiol. *50*, 1467–1476.

Murshudov, G.N., Vagin, A.A., and Dodson, E.J. (1997). Refinement of macromolecular structures by the maximum-likelihood method. Acta Crystallogr. *D53*, 240–255.

Nakamura, Y., and Ito, K. (2003). Making sense of mimic in translation termination. Trends Biochem. Sci. *28*, 99–105.

Perrakis, A., Morris, R., and Lamzin, V.S. (1999). Automated protein model building combined with iterative structure refinement. Nat. Struct. Biol. *6*, 458–463.

Petry, S., Brodersen, D.E., Murphy, F.V., Dunham, C.M., Selmer, M., Tarry, M.J., Kelley, A.C., and Ramakrishnan, V. (2005). Crystal structures of the ribosome in complex with release factors RF1 and RF2 bound to a cognate stop codon. Cell *123*, 1255–1266.

Rawat, U., Gao, H., Zavialov, A.V., Gursky, R., Ehrenberg, M., and Frank, J. (2006). Interactions of the release factor RF1 with the ribosome as revealed by cryo-EM. J. Mol. Biol. *357*, 1144–1153.

Rawat, U.B.S., Zavialov, A.V., Sengupta, J., Valle, M., Grassucci, R.A., Linde, J., Vestergaard, B., Ehrenberg, M., and Frank, J. (2003). A cryo-electron microscopic study of ribosome-bound termination factor RF2. Nature *421*, 87–90.

Remmers, A.E., Posner, R., and Neubig, R.R. (1994). Fluorescent guanine nucleotide analogs and G protein activation. J. Biol. Chem. *269*, 13771–13778.

Schuwirth, B.S., Borovinskaya, M.A., Hau, C.W., Zhang, W., Vila-Sanjurjo, A., Holton, J.M., and Cate, J.H. (2005). Structures of the bacterial ribosome at 3.5 A resolution. Science *310*, 827–834.

Scolnick, E., Tompkins, R., Caskey, T., and Nirenberg, M. (1968). Release factors differing in specificity for terminator codons. Proc. Natl. Acad. Sci. USA *61*, 768–774.

Shin, D., Brandsen, J., Jancarik, J., Yokota, H., Kim, R., and Kim, S.H. (2004). Structural analyses of peptide release factor 1 from Thermotoga maritima reveal domain flexibility required for its interaction with the ribosome. J. Mol. Biol. *341*, 227–239.

Song, H., Parsons, M.R., Rowsell, S., Leonard, G., and Phillips, S.E. (1999). Crystal structure of intact elongation factor EF-Tu from Escherichia coli in GDP conformation at 2.05 A resolution. J. Mol. Biol. *285*, 1245–1256.

Spahn, C.M.T., Blaha, G., Agrawal, R.K., Penczek, P., Grassucci, R.A., Trieber, C.A., Connell, S.R., Taylor, D.E., Nierhaus, K.H., and Frank, J. (2001). Localization of the ribosomal protection protein Tet(O) on the ribosome and the mechanism of tetracycline resistance. Mol. Cell *7*, 1037–1045.

Stansfield, I., Jones, K.M., Kushnirov, V.V., Dagkesamanskaya, A.R., Poznyakovski, A.I., Paushkin, S.V., Nierras, C.R., Cox, B.S., Ter Avanesyan, M.D., and Tuite, M.F. (1995). The products of the SUP45 (eRF1) and SUP35 genes interact to mediate translation termination in Saccharomyces cerevisiae. EMBO J. *14*, 4365–4373.

Stark, H., Rodnina, M.V., Rinke-Appel, J., Brimacombe, R., Wintermeyer, W., and van Heel, M. (1997). Visualization of elongation factor Tu on the Escherichia coli ribosome. Nature *389*, 403–406.

Tronrud, D.E., Ten Eyck, L.F., and Matthews, B.W. (1987). An efficient general-purpose least-squares refinement program for macromolecular structures. Acta Crystallogr. *A43*, 489–501.

Valle, M., Sengupta, J., Swami, K., Grassucci, R.A., Burkhardt, N., Nierhaus, K.H., Agrawal, R.K., and Frank, J. (2002). Cryo-EM reveals an active role for the aminoacyl-tRNA in the accommodation process. EMBO J. *21*, 3557–3567.

Valle, M., Zavialov, A.V., Sengupta, J., Rawat, U., Ehrenberg, M., and Frank, J. (2003). Locking and unlocking of ribosomal motions. Cell *114*, 123–134.

Vestergaard, B., Van, L.B., Andersen, G.R., Nyborg, J., Buckingham, R.H., and Kjeldgaard, M. (2001). Bacterial polypeptide release factor RF2 is structurally distinct from eukaryotic eRF1. Mol. Cell *8*, 1375–1382.

Vestergaard, B., Sanyal, S., Roessle, M., Mora, L., Buckingham, R.H., Kastrup, J.S., Gajhede, M., Svergun, D.I., and Ehrenberg, M. (2005). The SAXS solution structure of RF1 differs from its crystal structure and is similar to its ribosome bound cryo-EM structure. Mol. Cell *20*, 929–938.

Zavialov, A.V., and Ehrenberg, M. (2003). Peptidyl-tRNA regulates the GTPase activity of translation factors. Cell *114*, 113–122.

Zavialov, A.V., Buckingham, R.H., and Ehrenberg, M. (2001). A posttermination ribosomal complex is the guanine nucleotide exchange factor for peptide release factor RF3. Cell *107*, 115–124.

Zavialov, A.V., Mora, L., Buckingham, R.H., and Ehrenberg, M. (2002). Release of peptide promoted by the GGQ motif of class 1 release factors regulates the GTPase activity of RF3. Mol. Cell *10*, 789–798.

Zhang, B., Zhang, Y., Shacter, E., and Zheng, Y. (2005). Mechanism of the guanine nucleotide exchange reaction of Ras GTPase–evidence for a GTP/GDP displacement model. Biochemistry *44*, 2566–2576.

Zhouravleva, G., Frolova, L., Le, G.X., Le Guellec, R., Inge-Vechtomov, S., Kisselev, L., and Philippe, M. (1995). Termination of translation in eukaryotes is governed by two interacting polypeptide chain release factors, eRF1 and eRF3. EMBO J *14*, 4065–4072.